

RSC Advances



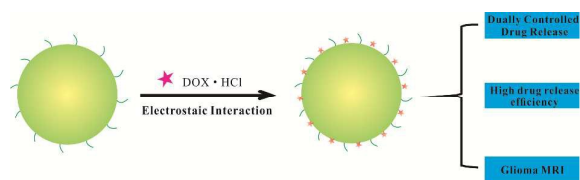
This is an *Accepted Manuscript*, which has been through the Royal Society of Chemistry peer review process and has been accepted for publication.

Accepted Manuscripts are published online shortly after acceptance, before technical editing, formatting and proof reading. Using this free service, authors can make their results available to the community, in citable form, before we publish the edited article. This *Accepted Manuscript* will be replaced by the edited, formatted and paginated article as soon as this is available.

You can find more information about *Accepted Manuscripts* in the [Information for Authors](#).

Please note that technical editing may introduce minor changes to the text and/or graphics, which may alter content. The journal's standard [Terms & Conditions](#) and the [Ethical guidelines](#) still apply. In no event shall the Royal Society of Chemistry be held responsible for any errors or omissions in this *Accepted Manuscript* or any consequences arising from the use of any information it contains.

Dually responsive polymeric particles for brain tumor (glioma) MR imaging and anticancer drug delivery.





Paramagnetic, pH and Temperature-sensitive Polymeric Particles for Anticancer Drug Delivery and Brain Tumor Magnetic Resonance Imaging

Received
Accepted

DOI: 10.1039/x0xx00000x

www.rsc.org/

Ruiqing Liu^{a,1}, Shuang Liang^{b,1}, Cun Jiang^a, Xin Wang^a, Ying Gong^a, Penghui Li^c, Zushun Xu^{a*}, Haibo Xu^{b*}, and Paul K. Chu^{c*}

Smart polymer-based theranostic agents often exist the problem of low drug release rate and are difficult to reach the site of brain tumors for magnetic resonance imaging (MRI). To synthesize a theranostic agent for brain tumor MRI with high drug release rate, a paramagnetic, pH and temperature-sensitive polymeric particle (PPP) is synthesized using simplified processes in this work. These dually sensitive polymeric particles show negligible cytotoxicity against HeLa and glioma (C6) cells. The obtained polymeric particles can effectively load anticancer drug doxorubicin (DOX). *In vitro* drug release measurements exhibit retarded release profile when subjected to varying pH or temperature. Moreover, DOX-loaded PPP exhibits obvious antitumor properties for C6 cells. The percentage of cumulative DOX release is higher than 95 % while both pH and temperature are changed. The T_1 -weighted relaxivity values at 3 T are 12.41 mM⁻¹ s⁻¹ (pH = 6.3) and 10.75 mM⁻¹ s⁻¹ (pH = 7.4). *In vivo* MRI reveals that the PPPs can be effectively imaged in brain tumor (glioma). These results indicate that the PPPs have great potential in diagnosing and treating glioma.

1. Introduction

Gliomas are the most common and aggressive intracranial tumors causing the central nervous system (CNS) cancers.^{1,2} Currently, cytoreductive surgery combining radiotherapy and chemotherapy is regarded as the most effective gliomas treatment. However, the chemotherapy drug is hard to concentrate on the diseased area, which may harm the normal issues. Moreover, how to accurately differentiate the normal neurological tissues with diseased tissues is a big challenge. MRI, owing to its excellent soft-tissue contrast properties,³ has

become a powerful neuroimaging technique and plays an important role in surgical glioma imaging.^{4,5} Theranostics, a platform combines diagnosis and therapy, has attracted increasing interests in recent years.⁶⁻⁸ Hence, a theranostic agent confining MRI, targeting drug delivery, and controlled release in one entity, which can diagnose and treat glioma without harming normal tissues, is of great significance

Stimuli responsive polymers have been suggested to be one of the most promising carriers of diagnostic and therapeutic agents.⁹⁻¹¹ Nevertheless, the polymer-based theranostic agent mentioned above is hard to reach the site glioma due to the blood tumor brain barriers (BTBB). An effective strategy to solve the problem is conjugating targeting receptors overexpressed on glioma cells to the polymeric theranostic agents.¹²⁻¹⁵ In contrast with the receptor-contained theranostic agent, those without receptor which can disrupt BTBB are more fascinating due to their easy availability.

pH and temperature are attractive stimulus utilized to control drug release as a result of tumor regions processing a more

^a.Hubei Collaborative Innovation Center for Advanced Organic Chemical Materials; Ministry of Education Key Laboratory for the Green Preparation and Application of Functional Materials, Hubei University, Wuhan, Hubei 430062, China. E-mail: zushunxu@hubei.edu.cn, Tel.: + 852 34427724; fax: + 852 34420542.

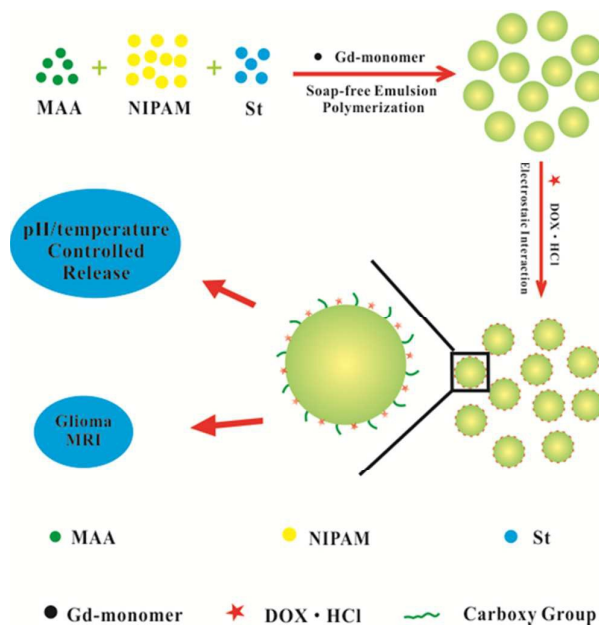
^b Department of Radiology, Union Hospital, Tongji Medical College, Huazhong University of Science and Technology, Wuhan, Hubei 430030, China. E-mail: xuhaibo1120@hotmail.com, Tel.: + 86 27 85726410; fax: + 86 27 85726919.

^c Department of Physics and Materials Science, City University of Hong Kong, Tat Chee Avenue, Kowloon, Hong Kong, China. E-mail: paul.chu@cityu.edu.hk, Tel.: + 86 27 88661897; fax: + 86 27 88665610.

¹ These two authors contributed equally to this work

acidic environment or a higher temperature.¹⁶ The control of drug release in most reported theranostic system is triggered by single stimuli such as pH or temperature.¹⁷⁻²⁰ However, compared with the single stimuli controlled release system, multi stimuli one can realize drug release when any stimuli responded to the system is changed, which may suggest us more choice to achieve real controlled drug release. What's more, dual stimuli controlled drug release platform may improve drug release efficiency which is important in improving the utilization of drugs. There are some reports related to polymer drug carrier for dual stimuli controlled drug release.^{21,22} Unfortunately, to the best of our knowledge, there are still no reports about receptor-free and dually responsive polymer theranostic agents for glioma diagnosis and therapy.

In order to prepare dually responsive polymeric theranostic agents with high drug release efficiency, hydrophilic stimuli responsive polymer should distribute in the outer space so that the loaded drug can easily escaped from polymeric particles, which can be realized by the copolymerization of hydrophobic monomer such as styrene with hydrophilic stimuli responsive polymer.²³ In addition, the introduced hydrophobic monomer may make a contribution to the affinity of receptor-free polymeric particles to glioma on account that hydrophobic polymers are easier recognized by proteins.²⁴ Hence, in this study, we first prepare paramagnetic, pH and temperature-sensitive polymeric particles (PPPs) using soap-free emulsion polymerization in the presence of methacrylic acid (pH-sensitive monomer), N-isopropylacrylamide (temperature-sensitive monomer), and hydrophobic styrene. Then load doxorubicin (DOX) to the PPPs. The obtained DOX-loaded PPP can be used as an effectively theranostic agents for pH/temperature-controlled drug release and glioma MRI (Scheme 1). The pH and temperature dual stimuli controlled drug release platform can achieve high drug release rate when both pH and temperature are changed. Furthermore, we find that the DOX-loaded polymeric particles without glioma cell-receptor can also traverse BTBB and reach to the site of glioma enhancing MRI.



Scheme 1. Illustration of the synthetic processes and formation of DOX-loaded PPPs.

2. Materials and methods

2.1 Materials

Methacrylic acid (MAA) was obtained from Aladdin. Styrene (St) and potassium peroxydisulfate (KPS) were purchased from Sinopharm Chemical Reagent Co. Ltd., China. Doxorubicin hydrochloride (DOX·HCl) was purchased from J&K Scientific. N-isopropylacrylamide (NIPAM, 99%) was purchased from Acros Organics. NIPAM and KPS were purified by recrystallization from a toluene/hexane mixture (v/v=1:1) and deionized water, respectively. St and MAA were purified by distillation under reduced pressure and stored at 2 °C. All the other reagents were analytical reagent (AR) and used as received.

2.2 Preparation of Paramagnetic, pH/temperature-responsive Polymeric Particles

Gd(III)-monomer was synthesized as the method developed in our previous work.²⁵ The PPPs were prepared by soap-free emulsion polymerization. Briefly, NIPAM (1.000 g), MAA (0.201 g), St (0.502 g), and KPS (0.150 g) were dispersed in 100 mL of deionized water, sonicated for minutes, and transferred to a 250 mL four-necked round-bottomed flask with a Teflon mechanical stirrer and condenser under flowing nitrogen. It was agitated vigorously at room temperature for 30

minutes under nitrogen and semitransparent dispersion was obtained. The solution was heated to 79 °C in a water bath and a series of Gd(III)-monomer water solution (Gd(III)-monomer contents 0, 0.025, 0.050, 0.075, 0.100, and 0.125 g, respectively) was added dropwise. The polymerization reaction lasted for 2.5 h at 79 °C under constant stirring and a series of PPPs (designated as PPP1 to PPP6) was obtained. The PPPs were dialyzed (cut-off $M_w = 14000$ Da) against distilled water for 5 days to remove unreacted monomers and other low molecular weight molecules. The distilled water was changed every 8 hours. To obtain solid samples, a saturated calcium chloride/methanol solution was added to latex followed with centrifugation at 4000 r min⁻¹. The precipitate was rinsed with distilled water three times and then dried under vacuum at 50 °C for 48 h.

2.3 Preparation of DOX-loaded PPP

The drug-loaded PPP was prepared by directly mixing DOX·HCl with polymer particles. Typically, 2.5 mL purified PPP5 emulsion (PPP5 25 mg) was diluted with 5 mL ultrapure water, followed by adding 15 mL DOX·HCl aqueous solution (DOX·HCl 5 mg) into the diluted polymer emulsion dropwise. The mixture reacted for overnight in dark at room temperature with constant stirring. The unloaded free drug was removed by dialysis using a dialysis bag (cutoff $M_w=14000$ Da) against 1000 mL pure water with stirring at a rate of 300 rpm. Pure water was refreshed for 8 times within 4 h (0.5 h each). The drug loading efficiency (DLE) and drug loading content (DLC) were calculated according to the equations:

$DLC (\%) = \text{weight of drug encapsulated in PPP} / \text{weight of polymer} \times 100\%$

$DLE (\%) = \text{weight of drug encapsulated in PPP} / \text{weight of drug in feed} \times 100\%$

The concentration of DOX·HCl in distilled water was obtained from calibration curve: $c (\mu\text{g/mL}) = (I - 0.08706) / 0.01630$ ($R^2 = 0.9998$),¹⁷ where I is the UV absorption intensity at 485 nm obtained by subtracting the UV absorbance of the pure PPP solution from that of the DOX-loaded PPP.

2.4 In Vitro Drug Release Measurements

The DOX-loaded PPP after removing free DOX·HCl was divided into several parts, which were put into six new dialysis tubes immediately to evaluate the drug release behavior. The

drug release process was carried out by dialyzing 3.0 mL of DOX-loaded PPP in the dialysis tube (cut-off $M_n = 8000-10000$ Da) against 150 mL of tris-buffer (0.01 M; pH 5.0, pH 7.4) in a beaker (200 mL), 250 rpm of stirring rate, the six tubes were divided into three groups and the temperature was kept at 25 °C, 37 °C, and 43 °C, respectively. At desired time intervals, 3.0 mL buffer in the beaker was removed for fluorescence spectroscopy (excitation at 461 nm and emission at 591 nm) and the cumulative release curve of DOX was obtained. The volume of the buffer outside of the dialysis tube in the beaker was ensured around 150 mL during the measurement.

2.5 Cytotoxicity Assessment

The cytotoxicity of the PPP, DOX-loaded PPP, and free DOX against HeLa cells and glioma cancer (C6) cells were evaluated by typical 3-(4, 5-dimethylthiazol-2-yl)-2, 5-diphenyltetrazoliumbromide (MTT) assay. HeLa and C6 cells were seeded in a 96-well cell culture plate at a density of 1×10^4 cells per well and incubated at 37 °C for 24 h under 5% CO₂ humid atmosphere. The medium was then replaced by PPP, DOX-loaded PPP, or free DOX solution at different concentrations and subsequently incubated for another 48 h. Untreated cells were served as control groups. After incubated for 48 h, MTT (20 μL, 5 mg mL⁻¹) was added to each well incubated for 4 h. The growth medium was removed and 150 μL DMSO was added to each well. The optical density (OD) was measured at 490 nm using microplate reader (Rayto Rt2100c). The relative cell viability (%) was determined by the comparing OD of experimental group with control group.

2.6 In vitro T_1 -weighted MR imaging

The longitudinal relaxation rates ($1/T_1$) of PPPs in tris-buffer (0.01M) with variable gadolinium concentrations (0.025, 0.05, 0.1, 0.2, and 0.4 mM) at pH value of 6.3 and 7.4 were determined at room temperature using the Siemens Magnetom Trio 3.0 T whole-body MR scanner. The spin-echo pulse sequence was used in the T_1 measurements using the following parameters: Field of view (FOV) = 10×10 cm; Echo time (TE) = 9 ms; Slice thickness = 3 mm. The repetition time (TR) was 300, 400, 500, 600, 800, 1000, 2000, and 3000 ms. The samples were set on a 96-well plate under the MR scanner to get different T_1 and a linear fit was applied to $1/T_1$ versus Gd(III) concentrations to estimate the longitudinal relaxation rates (r_1).

2.7 Experimental animals

Several adult male Sprague-Dawley (SD) rats weighing approximately 250 g were used *in vivo* glioma MRI. All the animals were managed and treated according to the rules and regulations of the Institutional Animal Care and Use Committee at Hubei University. Rats tumor xenografts were established by solid orientation method injection of C6 glioma cancer cells with 1×10^6 cells per bregma. After 15 days of tumor xenografts, the glioma tumor bearing rats were used for MRI investigations.

2.8 In Vivo T_1 -Weighted Brain Tumor MRI and Biodistribution Study

Glioma xenografts bearing rats ($n=6$) were employed for *in vivo* MRI. Rats (dosage $0.05 \text{ mmol Gd Kg}^{-1}$) were injected with PPP by tail vein and scanned on the 3.0 T Siemens Magnetom Trio clinical MRI scanner. The T_1 -weighted images of brain were taken at various time points (0 min, 30 min, 1 h, 2 h, 3 h, and 6 h) with TE/TR = 10/0.44, thickness = 3 mm, and averages = 6 using spin-echo pulse sequence. Three rats were sacrificed at 120 min post-injection for biodistribution study. The organ and tissue samples of the liver, spleen, heart, lung, kidneys, brain (tumor), and muscle were collected and weighed. The samples were then cut into pieces and treated with 65 % nitric acid and filtered. The gadolinium concentration in the filtrate was determined by ICP-OES and calculated as the percentage of injected dose per gram of organ/tissues (% ID/g).

2.9 Characterization of PPPs

The Gd(III)-monomer and PPPs were characterized by Fourier transform infrared spectroscopy (FT-IR, Nicolet iS50 Thermofisher USA) after the dried samples were pressed with KBr into compact pellets. The gadolinium concentration was determined by inductively-coupled plasma optical emission spectrometry (ICP-OES, Optimal 8000 PE. USA). The morphology of the PPPs was examined by transmission electron microscopy (TEM, Tecnai G20, FEI Corp. USA, at 200 kV) and scanning electron microscopy (SEM, JSM6510LV, JEOL, Japan). Prior to conducting TEM, the samples were dispersed on amorphous carbon coated copper grids. The SEM samples were prepared by dropping the emulsion onto glass slides and dried at room temperature. The glass slides were then vacuum coated with a thin gold film. The hydrodynamic

diameter, size distribution, and zeta potential were measured on the Zetasizer (ZS90, Malvern UK.). The thermal stability of the PPPs was assessed on the Perkin-Elmer TGA-7 between 30 °C and 600 °C at a heating rate of 20 °C per minute. The fluorescent spectra were acquired on the LS-55 spectrometer (PE, USA).

3. Results and Discussion

3.1 Synthesis and Characterization of PPPs

The PPPs are synthesized by soap-free emulsion polymerization. Their chemical structure can be determined by FT-IR spectrum. As shown in Fig. 1b and 1c, the O-H and N-H stretch vibration absorption peaks can be observed at 3401 cm^{-1} and 3300 cm^{-1} respectively. The peaks at 2973 cm^{-1} , 2925 cm^{-1} , and 2883 cm^{-1} can be assigned to the asymmetrical and symmetrical stretching of $-\text{CH}_3$ and $-\text{CH}_2$, respectively. The two peaks at 1578 cm^{-1} and 1545 cm^{-1} are the symmetrical stretching of O-C=O in PMAA. Moreover, the characteristic stretch absorption peak of C=O at 1706 cm^{-1} from carboxyl groups indicating the polymerization of MAA. The polymerization of NIPAM can be confirmed by the peaks at 1386 cm^{-1} and 1367 cm^{-1} corresponded to isopropyl groups. The peaks at 3033 cm^{-1} and 702 cm^{-1} are related to stretching and flexural vibration ($\delta_{\text{C-H}}$) of the benzene ring indicating the polymerization of St. The weak peak of Gd-N at 550 cm^{-1} indicates the Gd(III)-monomer (Fig. 1a and 1c), the other Gd(III)-monomer bonds are either too weak or overlapped in the spectrum. FT-IR spectra indicates that the NIPAM, MAA, St, and Gd(III)-monomer are polymerized.

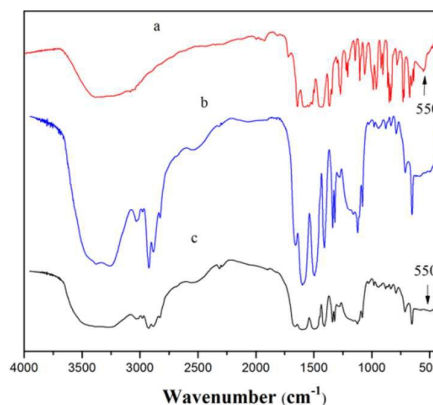


Fig. 1. FT-IR spectra of PPPs: (a) Gd(III)-monomer; (b) PPP1 without Gd(III)-monomer, and (c) PPP5 (the content of Gd(III)-monomer in PPP5 is 0.1 g).

3.2 Morphology and Particle Size

Particle size is an important factor for receptor-free probes to disrupt the BTBB of orthotopic xenograft glioma. Only the particle whose size lower than that of orthotopic xenograft glioma (200-1200 nm) can go through BTBB.²⁶ The morphology and particle size are determined by TEM, SEM, and dynamic light scattering (DLS). The TEM images and SEM image (PPP5) in Fig. 2 reveal the monodispersed morphology. Additionally, SEM image (Fig. 2e) indicates the PPP5 with a structure similar to core-shell because hydrophilic polymers which have low image contrast distribute in the outer space. PPP1, PPP3, and PPP4 (Fig. 2a-2c) have a diameter of about 200 nm under dry condition, whereas the diameter of PPP5 (Fig. 2d and 2e) is about 240 nm under the same condition. The hydrodynamic diameters (D_h) of PPP1 to PPP5 at 25 °C are 258.4 nm, 240.3 nm, 237.8 nm, 215.1 nm, and 277.9 nm, respectively. The PDI values are all below 0.1, suggesting monodispersity consistent with TEM and SEM. The diameter in an aqueous system is larger than that under dry condition due to the hydrophilic properties and swelling of the polymeric particles in water. The D_h value of the particles decreases with increasing Gd(III)-monomer (0-0.075 g) attributable cross-linking of the Gd(III)-monomer with three double bonds. The particles shrink when they are copolymerized with other monomers. However, for Gd(III)-monomer over than 0.075 g, the polymers are over cross-linked and D_h of PPP5 increases by about 20 nm compared to PPP1. No stable emulsion is observed from PPP6. Those results indicate that the PPPs with such size range are suitable for glioma MRI and the core-shell like structure may endow the PPPs high drug release efficiency.

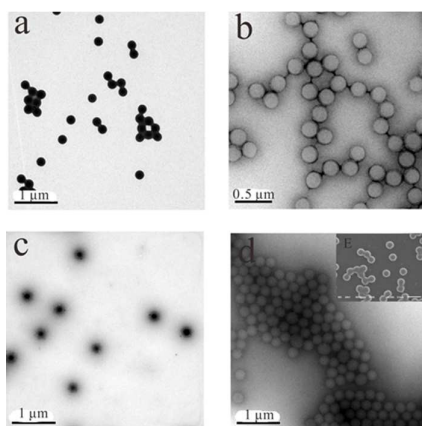


Fig. 2. TEM images of (a) PPP1, (b) PPP3, (c) PPP4, and (d) PPP5; (e) SEM image of PPP5.

3.3 pH and Temperature Sensitivity

The pH-dependent properties of the PPPs are investigated by dynamic light scattering (DLS). As shown in Fig. 3, when the pH is increased from 2 to 8, the hydrodynamic diameter (D_h) of the PPPs change by about 50 nm because of variations in hydrogen bonds and ionization of carboxyl groups. At a low pH (< 4), because of strong hydrogen bonds between the polymeric molecules and intramolecular hydrogen bonds of macromolecules, the polymer chains entangle with each other and smaller particles are formed. In contrast, as the pH is increased and becomes higher than the reported pK_a value of PMAA (~ 6),^{27, 28} the carboxyl groups are ionized and hydrogen bonds decrease. The polymer particles become more hydrophilic and swollen, resulting in a larger particle size.²⁹ These results indicate the good pH-sensitive property of PPPs.

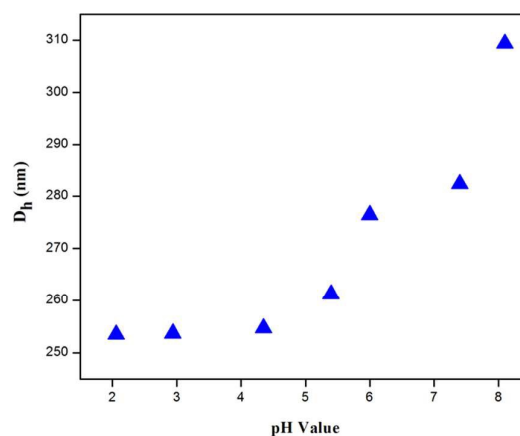


Fig. 3. Hydrodynamic diameters of the PPP5 as a function of pH.

The temperature dependence is assessed by DLS between 25 °C and 43 °C. As the temperature is increased, the particle shrinks as shown in Fig. 4 due to the change in the wettability of the polymers in the aqueous system. When the temperature is above the lower critical solution temperature (LCST) of PNIPAM (~ 32 °C), reduction in hydrogen bonds collapses the polymeric particles and the system transforms to globules.^{30, 31} The temperature sensitivity of PPP5 is better than that of PPP1 because the Gd(III)-monomer polymerizes with other monomers. The hydrophilic ability of the Gd(III)-monomer copolymers (PPP5) is better than that of the Gd(III)-monomer free copolymers (PPP1) due to the carboxylate groups in the Gd(III)-monomer. There are more hydrogen bonds in the

aqueous system of PPP5 below the LCST and more hydrogen bonds are disrupted when the temperature is above the LCST. The sizes of the PPPs change with varying temperature demonstrating their temperature-sensitive property.

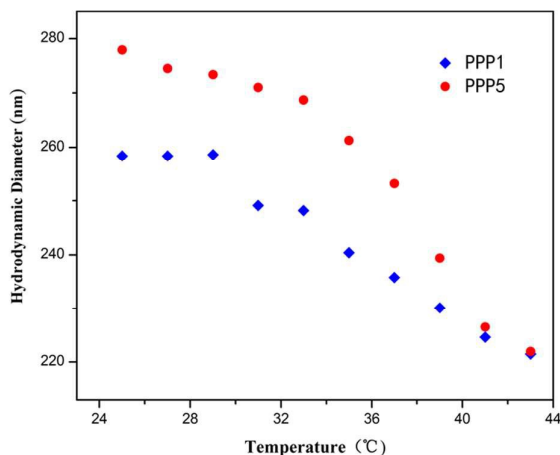


Fig. 4. Hydrodynamic diameters of PPP1 and PPP5 between 25 °C and 43 °C.

3.4 Stability of PPPs

Stability has great influence on the biotoxicity of gadolinium-based MRI contrast agents and good stability is indispensable for their biomedical applications. pH and temperature are two key factors affecting the stability of our PPPs. The pH-stability of PPP5 is evaluated by DLS and ICP-OES. The PPP5 emulsion is dialyzed against an aqueous solution at pH of 4.0 and 8.5 for 5 days and the free Gd(III) ions released from the PPP5 are determined by ICP-OES. There are negligible free Gd(III) ions released from the polymeric particles. The zeta potentials of the dialyzed PPP5 at pH of 4.0 and 8.5 are -36.8 mV and -48.4 mV, respectively, suggesting the PPPs are stable in this pH range.

The thermal stability of the PPPs is evaluated by thermogravimetric analysis (TGA). As shown in Fig. 5, the 7.4 % loss in weight percentage near 100 °C corresponds to loss of bound water from PPPs and the sharp weight loss from 365 °C to 430 °C is related to decomposition of the polymer backbone. The last weight loss stage in the TGA curves over 430 °C corresponds to the residual weight of gadolinium existing as oxide. There are no residual weight percentage for PPP1 at 600 °C and the residual weight percentage of PPP5 at 600 °C is about 1.2 %.

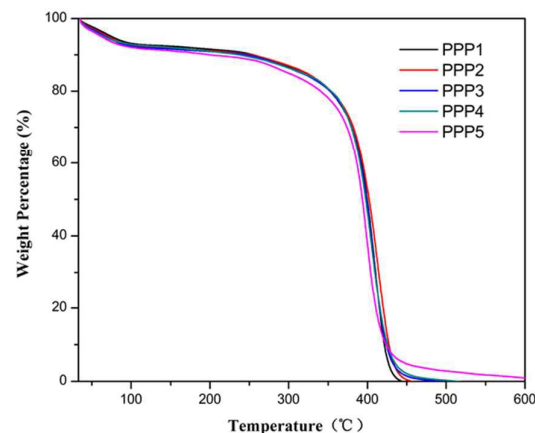


Fig. 5. TGA curves of PPPs acquired between 30 and 600 °C at a heating rate of 20 °C per minute.

3.5 DOX-Loading and *In Vitro* Release Profiles of PPP

For the purpose of evaluating the potential application of PPP as a drug delivery vehicle, DOX loading and release were both studied with different pH values and temperatures. The DLC and DLE are determined by subtracting the UV absorbance of the PPP from DOX-loaded PPP at 485 nm. The electrostatic interactions between $-\text{COO}^-$ groups of PMAA and $-\text{NH}_3^+$ of $\text{DOX}\cdot\text{HCl}$ drive the loading process. The drug loading content is about 16.1 wt % and the DLE is about 80.4 wt %, the DLE is higher than that of the most reported drug delivery systems including polymers.³² In addition, the DOX concentration in the solution is about $150 \mu\text{g mL}^{-1}$. The *in vitro* release profiles of DOX-loaded PPP are shown in Fig. 6. First, to investigate pH-triggered DOX release behavior of the PPPs, two pH values similar to blood and tumor region are selected. As shown in Fig. 6a, the percentages of cumulative DOX release decrease with increased pH. After dialyzing for 53 h, when the temperature is fixed at 37 °C, 92.9 % drugs release from PPP at pH=5.0, which is 2.5 times higher than that of pH at 7.4 (36.3 %). This can be attributed to the protonation of the $-\text{COO}^-$ groups in the PAA chains at pH 5.0 accelerating the DOX ($pK_{\text{a}}^{\text{DOX}\cdot\text{HCl}}=8.25$)³³ release from the polymeric particle corona. The pH-sensitive drug release behavior is significant in practical applications because of the more acidic environment of tumor sites than that of the normal ones

Additionally, we also investigate the temperature-sensitive release performance of the PPPs. Three temperature below

(25 °C), around (37 °C), and above (43 °C) human normal temperature are chosen while pH value is kept at 5.0. The DOX release rate at 43 °C and 37 °C are 20.9 % and 8.8 % higher than that of 25 °C, respectively (Fig. 6b). It is because 25 °C is lower than the LSCT of PPPs (~ 32 °C). With the increasing of the temperature, polymeric particle shrunk which facilitate the release of drug due to the surface area of particle decrease. The size of PPP at 43 °C decreases heavily compared with that at 37 °C, thus, a higher release percentage can be obtained. The above results indicate the temperature-sensitive releasing property of PPPs.

Moreover, we investigate pH and temperature dual stimuli triggered releasing property of the PPP. Owing to that tumor regions generally exhibit a more acidic or a higher temperature environment,¹⁶ we optimize pH=7.4 at 25 °C and pH=5.0 at 43 °C as comparison. As shown in Fig. 6c, when pH decreases from 7.4 to 5.0 simultaneously temperature increases from 25 °C to 43 °C, the percentage of cumulative DOX release improves

65.9 % and reaches to 96.3 %, which is much higher than that of the reported single stimuli controlled drug release systems,^{17, 18, 34} and also higher than that of the reported poly(NIPAM-MAA-ODA) system (ODA= Octadecyl acrylate).²² The high release percentage can be attributed to the coaction of pH and temperature. At higher temperature, polymeric particle shrunk simultaneously electrostatic interactions between polymer particles and drugs are disrupted when pH changes. In addition, after the electrostatic interactions are broken, no barrier interfere the release of drugs due to -COO⁻ groups in such copolymers distributed in the outer space.³⁵ The results indicate that both pH and temperature can dominate the release of DOX. More importantly, compared with single stimuli triggered drug delivery system, dual stimuli triggered drug release systems own high percentage of DOX release which is very important in improving utilization of drugs and lowering the cost of therapy. Moreover, dual stimuli triggered platform is more flexible to realize controllable drug release owing to its multi-responsive property.

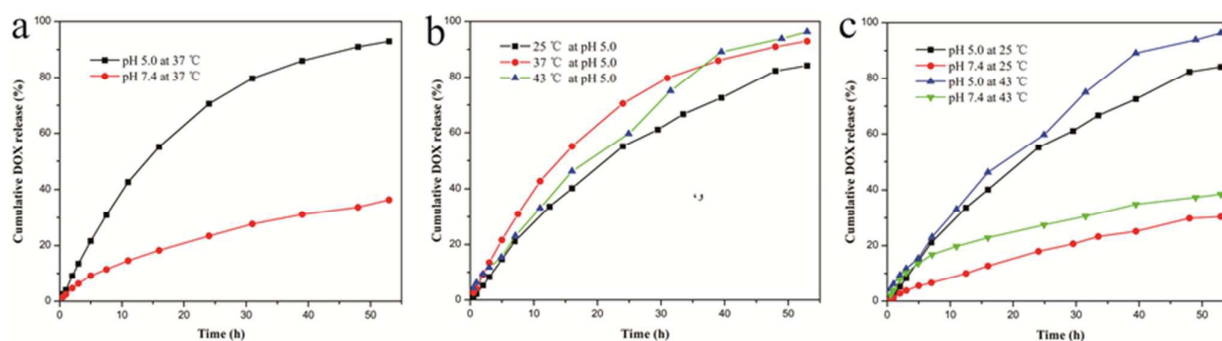


Fig. 6. Cumulative drug release profiles of DOX-loaded PPPs in tris-buffer (0.01M), (a) pH- controlled release at 37 °C, (b) Temperature controlled release at pH 5.0, and (c) pH and temperature dually controlled release.

3.6 Cytotoxicity of PPPs

The cytotoxicity of the PPP is an important factor for their *in vivo* applications and is evaluated by standard MTT against HeLa and C6 cells. The PPP at various concentrations is incubated with HeLa and C6 cells for 48 hours and the relative cell viability is calculated by measuring the optical density. The PPP shows excellent cytocompatibility in the concentration range and all the relative cell viability is above 80 % (Fig. 7). The good biocompatibility can be ascribed to the good stability of the PPPs and biocompatibility of the polymers, particularly the synthetic method employed here as no toxic organic solvents and emulsifiers are used.

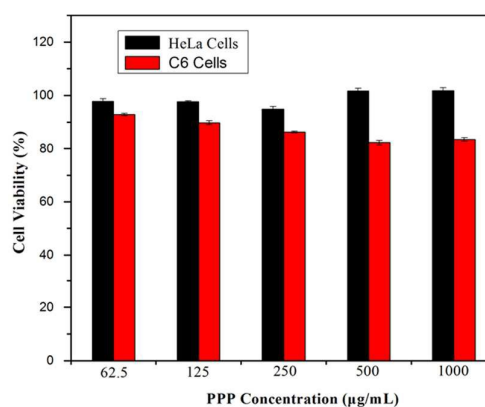


Fig. 7. Cell viability against HeLa and C6 cells assessed by MTT assay.

3.7 Antitumor Properties of DOX-Loaded PPP

For further applications in biomedical field, it is necessary to study the antitumor property. The *in vitro* antitumor properties of DOX-loaded PPP are studied on HeLa and C6 cells via cell viability assay with free DOX as control. As illustrated in Fig. 8, cell viability decreases significantly when HeLa or C6 cells are treated with DOX-loaded PPP. The proper concentration of DOX to realize effective therapy (cell viability of cells is less than 40 %) should be more than $5 \mu\text{g mL}^{-1}$. Furthermore, the DLC of PPP5 is 16.1 wt % and drug release rate is more than 90 %. Hence, the final concentration of DOX released from PPP can reach to $135 \mu\text{g mL}^{-1}$, which is much higher than essential concentration $5 \mu\text{g mL}^{-1}$. However, when DOX concentration is higher than $40 \mu\text{g mL}^{-1}$, the cell viability of HeLa cells is still near 49 % (Fig. 8a), while C6 cells are only 27 % (Fig. 8b). The result demonstrates the antitumor ability of DOX-loaded PPP for C6 cells is better than that for HeLa cells, indicating good affinity of DOX-loaded PPP for C6 cells. While the cells are treated with DOX-loaded PPP, C6 cells capture more DOX-loaded PPP and larger amount of drugs are in the cells resulting lower cell viability. The good biocompatibility of PPP and effective antitumor ability of DOX-loaded PPPs make the biomedical applications possible.

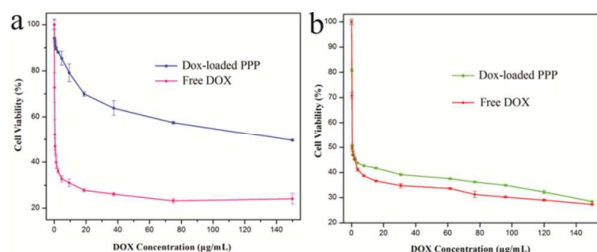


Fig. 8. Antitumor activities of DOX-loaded PPP against (a) HeLa cells and (b) C6 cells via cell viability assay with free DOX as control.

3.8 Relaxivity of PPPs

To assess the paramagnetic sensitivity of the PPPs, the longitudinal relaxation time (τ_1) of water protons in PPP5 is measured on a clinical 3.0 T MR scanner at various Gd(III) concentrations. The pH values of the PPP5 dispersion are 6.3 and 7.4, respectively. The relaxivity is $12.41 \text{ mM}^{-1} \text{ s}^{-1}$ at pH value of 6.3 and $10.75 \text{ mM}^{-1} \text{ s}^{-1}$ at pH value of 7.4, as shown in Fig. 9. As the pH is decreased from 7.4 to 6.3, larger relaxivity is observed, indicating that protonation of the carboxyl groups in PPP5 under acidic conditions renders the water molecules more accessible to the Gd(III) center.^{36, 37} The r_1 of PPP is about 2 times higher than Magnevist® (about $r_1=4.4 \text{ mM}^{-1} \text{ s}^{-1}$). In particular, the relaxivity is pH-dependent, which is significant in the diagnosis of tumors due to their acidic

environment. The high relaxivity can be attributed to two reasons. The hydrophilic PMAA and PNIPAM in the particles improve the rotational correlation time (τ_r) and water exchange rates (τ_m) based on the SBM theory.³⁸ The improved τ_r and τ_m lead to high relaxivity. Moreover, there are plenty of Gd(III) centers in the polymeric particles and the multiple center of Gd(III) in the paramagnetic particles can also contribute to the high relaxivity of the PPPs.³⁹

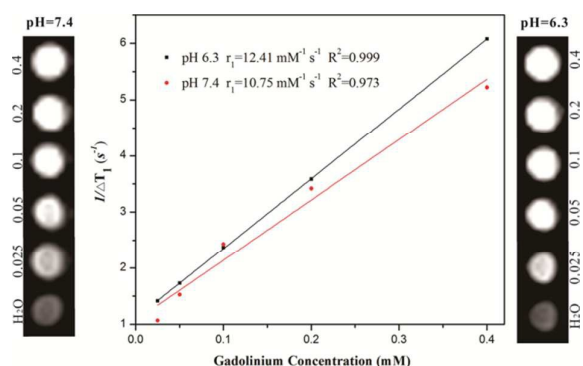


Fig. 9. T_1 -weighted relaxivity of PPP5. The longitudinal relaxation time (T_1) is measured on a clinical 3.0 T MR scanner at various Gd(III) concentrations at pH 6.3 and 7.4.

3.9 In Vivo Brain Tumor MRI

To explore the specificity of the PPPs and whether they are effective in brain tumor imaging, MRI is carried out on glioma-bearing SD mice. The T_1 -weighed MR images of the brain tumor are obtained at several time points. The organs/tissues are collected from the glioma loaded mouse 120 min after tail vein injection of the PPPs for biodistribution analysis. The amount of gadolinium in the organs/tissues is determined by ICP-OES and presented as percentage of injected dose per gram of organ/tissues. As shown in Fig. 10, after 0.5 h post-injection, the PPPs show effective brain tumor (glioma) contrast enhancement. At 6 h post-injection, the PPP still shows obvious enhancement of MRI.

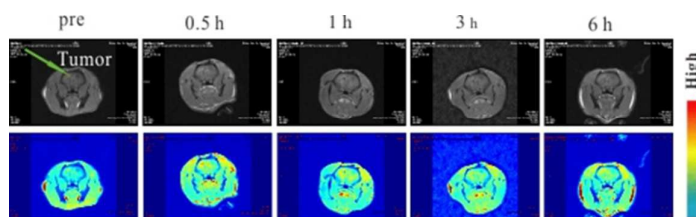


Fig. 10. T_1 -weighted glioma-bearing rats MR images taken at time points of 0, 15, 60, 180, and 360 min.

Moreover, the biodistribution tests indicate the gadolinium in brain tumor is the largest (27 %) (Fig. 11), suggesting that the PPPs are brain tumor inveterate. This can be attributed to the special environment of glioma. Some proteins such as β -catenin which is indispensable in the formation of glioma are overexpressed.¹ Those proteins may show specific affinity to carboxyl groups contained polymers. The $-\text{COO}^-$ groups in the PPPs which distributed in the outer space can react with amino groups in the proteins directly. What's more, the diameter of the PPP is about 270 nm. Vehicle with the size ranging from 200 to 1200 nm can disrupt blood brain tumor barrier and be captured by glioma through enhanced permeability and retention (EPR) effect.^{5, 26, 40} Additionally, the copolymerization of hydrophobic St may also make a contribution to the capture of PPP by glioma. Those results are of great significance in the diagnosis and treatment of brain tumors.

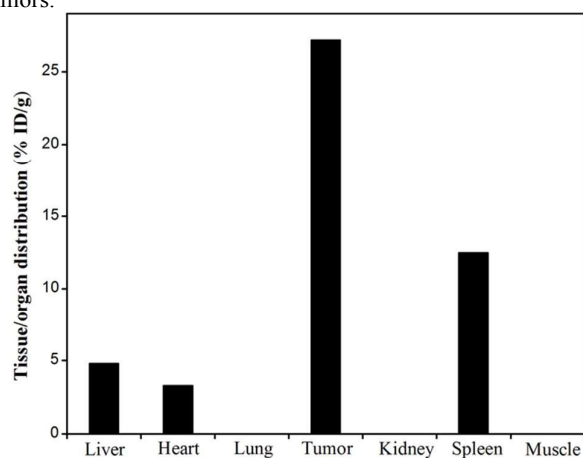


Fig. 11. In vivo biodistribution of PPP. The organs/tissues are collected from the glioma loaded rats after 120 min tail-vein of PPP. The PPP content is determined by ICP-OES and presented as the percentage injected dose accumulated per mass unit of organ/tissue (% ID/g).

4. Conclusions

Paramagnetic particles sensitive to pH and temperature are prepared by soap-free polymerization. The PPPs having a hydrodynamic diameter of about 250 nm are monodispersed (PPP5 is 270 nm) and have excellent stability at different pH values. The excellent stability, DOX loading ability, good biocompatibility, pH/temperature controlled drug release property, effective antitumor properties, and brain tumor (glioma) MR imaging capability of the PPPs render them highly suitable for controlled drug delivery to brain tumors. Significantly, the high drug release efficiency can improve the utilization of antitumor drugs which is very important for lowering the cost of treatment. Furthermore, we find that the receptor-free polymeric particles can also disrupt BTBB for

brain tumor MRI, which may suggest us a new choice to fabricate agents for diagnosing and treating brain tumors.

Acknowledgements

This work was supported by the National Natural Science Foundation of China (Grant NO. 51273058, 81171386, 81372369). This work was supported, in part, by Hong Kong Research Grants Council (RGC) General Research Funds (GRF) No. CityU 112212.

References

- 1 J. T. Huse and E. C. Holland, *Nat. Rev. Cancer.*, 2010, **10**, 319-331.
- 2 D. Krex, B. Klink, C. Hartmann, A. von Deimling, T. Pietsch, M. Simon, M. Sabel, J. P. Steinbach, O. Heese, G. Reifenberger, M. Weller and G. Schackert, *Brain : a journal of neurology*, 2007, **130**, 2596-2606.
- 3 M. Rudin and R. Weissleder, *Nat. Rev. Drug. Discov.*, 2003, **2**, 123-131.
- 4 E. A. Van Vliet, W. M. Otte, J. A. Gorter, R. M. Dijkhuizen and W. J. Wadman, *Neurobiol. Dis.*, 2014, **63**, 74-84.
- 5 X. Gao and C. Li, *Small*, 2014, **10**, 426-440.
- 6 L. Twan, A. Silvio, E. H. Wim, S. Gert and K. Fabian, *Acc. Chem. Res.*, 2011, **44**, 1029-1038.
- 7 Y. Zhang, H. F. Chan and K. W. Leong, *Adv. Drug. Deliv. Rev.*, 2013, **65**, 104-120.
- 8 G. Biana, T. Ennio, X. W. Liu, E. S. Rita and F. Mauro, *Acc. Chem. Res.*, 2011, **44**, 979-989.
- 9 T. Krasia-Christoforou and T. K. Georgiou, *J. Mater. Chem. B*, 2013, **1**, 3002-3025.
- 10 A. K. Bajpai, S. K. Shukla, S. Bhanu and S. Kankane, *Prog. Polym. Sci.*, 2008, **33**, 1088-1118.
- 11 L. C. Ho, C. H. Hsu, C. M. Ou, C. W. Wang, T. P. Liu, L. P. Hwang, Y. Y. Lin and H. T. Chang, *Biomaterials*, 2015, **37**, 436-446.
- 12 R. Huang, L. Han, J. Li, S. Liu, K. Shao, Y. Kuang, X. Hu, X. Wang, H. Lei and C. Jiang, *Biomaterials*, 2011, **32**, 5177-5186.
- 13 D. Zhang, X. Y. Feng, T. D. Henning, L. Wen, W. Y. Lu, H. Pan, X. Wu and L. G. Zou, *Eur. J. Radiol.*, 2009, **70**, 180-189.
- 14 J. Li, S. Huang, K. Shao, Y. Liu, S. An, Y. Kuang, Y. Guo, H. Ma, X. Wang and C. Jiang, *Sci. Rep.*, 2013, **3**, 1623.
- 15 D. Ni, J. Zhang, W. Bu, H. Xing, F. Han, Q. Xiao, Z. Yao, F. Chen, Q. He, J. Liu, S. Zhang, W. Fan, L. Zhou, W. Peng and J. Shi, *ACS nano*, 2014, **8**, 1231-1242.
- 16 D. Schmaljohann, *Advanced drug delivery reviews*, 2006, **58**, 1655-1670.
- 17 Q. Liu, S. Chen, J. Chen and J. Du, *Macromolecules*, 2015, **48**, 739-749.

- 18 Q. Liu, H. Zhu, J. Qin, H. Dong and J. Du, *Biomacromolecules*, 2014, **15**, 1586-1592.
- 19 L. Zhou, X. Zheng, Z. Gu, W. Yin, X. Zhang, L. Ruan, Y. Yang, Z. Hu and Y. Zhao, *Biomaterials*, 2014, **35**, 7666-7678.
- 20 Y. Li, G. H. Gao and D. S. Lee, *Advanced healthcare materials*, 2013, **2**, 388-417.
- 21 R. Salehi, S. Rasouli and H. Hamishehkar, *Int. J. Pharm.*, 2015, **487**, 274-284.
- 22 X. Wu, Z. Wang, D. Zhu, S. Zong, L. Yang, Y. Zhong and Y. Cui, *ACS applied materials & interfaces*, 2013, **5**, 10895-10903.
- 23 S. Schmidt, T. Liu, S. Rütten, K.-H. Phan, M. Möller and W. Richtering, *Langmuir*, 2011, **27**, 9801-9806.
- 24 J. Moselhy, X. Y. Wu, R. Nicholov and K. Kodaria, *J. Biomater. Sci. Polym. Ed.*, 2000, **11**, 123-147.
- 25 *China Pat.*, CN 104672258 A, 2015.
- 26 K. H. Susan, L. M. Wayne, Y. Fan, R. W. Gregory, G. Linda, P. T. Vladimir and K. J. Rakesh, *Proc. Natl. Acad. Sci.*, 1998, **95**, 4607-4612.
- 27 K. Eugenia and A. S. Svetlana, *Macromolecules*, 2003, **36**, 9950-9956.
- 28 S. B. Rahane, J. A. Floyd, A. T. Metters and S. M. Kilbey, *Adv. Funct. Mater.*, 2008, **18**, 1232-1240.
- 29 J. Kost and R. Langer, *Adv. Drug. Deliv. Rev.*, 2012, **64**, 327-341.
- 30 A. Chan, R. P. Orme, R. A. Fricker and P. Roach, *Adv. Drug. Deliv. Rev.*, 2013, **65**, 497-514.
- 31 H. Zhu, J. Tao, W. Wang, Y. Zhou, P. Li, Z. Li, K. Yan, S. Wu, K. W. Yeung, Z. Xu, H. Xu and P. K. Chu, *Biomaterials*, 2013, **34**, 2296-2306.
- 32 X. Li, Y. Qian, T. Liu, X. Hu, G. Zhang, Y. You and S. Liu, *Biomaterials*, 2011, **32**, 6595-6605.
- 33 C. Amira, L. S. Patrick and E. Adi, *Langmuir*, 2005, **21**, 9308-9313.
- 34 Y. T. Chiang and C. L. Lo, *Biomaterials*, 2014, **35**, 5414-5424.
- 35 R. P. Todd Hoare, *Langmuir*, 2004, **20**, 2123-2133.
- 36 P. Caravan, *Chem. Soc. Rev.*, 2006, **35**, 512.
- 37 K. S. Kim, W. Park, J. Hu, Y. H. Bae and K. Na, *Biomaterials*, 2014, **35**, 337-343.
- 38 C. Peter, J. E. Jeffrey, J. M. Thomas and B. L. Randall, *Chem. Rev.*, 1999, **99**, 2293-2352.
- 39 C. Shen and E. J. New, *Curr. Opin. Chem. Biol.*, 2013, **17**, 158-166.
- 40 H. Sarin, A. S. Kanevsky, H. Wu, A. A. Sousa, C. M. Wilson, M. A. Aronova, G. L. Griffiths, R. D. Leapman and H. Q. Vo, *J. Transl. Med.*, 2009, **7**, 1-13.